

Dynamic Analysis of Rotating Continuous Drive Friction Welding Joints of Al alloy (6061AA)

Mamdouh I. Elamy^{1,2}

¹ Industrial Engineering Department, Northern Border University, Arar, Saudi Arabia

² Production Engineering & Mechanical Design Department, Menoufia University, Shebin El-Kom, Menoufia, Egypt

mamdouhelimi2017@gmail.com, Mamdouh.Morsi@nbu.edu.sa

ABSTRACT

A rotating Continuous Drive Friction Welding (CDFW) is a solidity welding process, where the required heat for welding is produced by friction induced by the relative movement between a motionless part and its rotary counterpart. In the situation of aluminum alloy, grain coarsening and impurities redistribution on grain boundaries are the main problems during fusion welding, which may be partially avoided via rotary friction welding.

The current research attempts to study the influences of time, rotational speed, and applied force on the dynamic analysis of rotating (CDFW) joints for aluminum alloy (6061AA). Numerical methods use finite element models with unified mechanical properties, which are incorporated into a welded joint structure and used to calculate Eigen-parameters quickly. Two techniques are used in the experimental analysis. The first one uses Frequency Response Function (FRF) applied with the impact hammering test, while the second one utilizes the magneto strictive pulse-echo delay line for the characterization of friction welded joints.

The assortment of numerical and experimental techniques makes it possible to find an effective tool for studying the dynamic performance of rotating CDFW joints for an aluminum rod. The proposed model was found to be capable of operating at high speeds while avoiding the resonance state utilizing the Finite Element Modeling (FEM) and the results from the experiments. The results showed that the change in applied force has the greatest influence on the dynamic performance of the continuous drive friction welding joints.

Keywords: Dynamic analysis; rotating continuous drive friction welded joint; finite element modeling; frequency response function (FRF)

1. Introduction

Friction welding (FW) is a method for joining solid materials. A few variations of friction welding include Friction Stir Welding (FSW), Friction Stir Spot Welding (FSSW), and Rotational Friction Welding (RFW). Continuous Drive Friction Welding (CDFW) is a form of RFW used to join rods and tubes of similar and dissimilar materials. Such welding techniques allow the materials to be joined without reaching the melting temperature and prevent the formation of intermetallic layers in similar material welding.

Frictional welding, commonly known as rotatory friction welding (RFW), is a solid-state weld method in which heat is generated by friction between rotating and stationary parts. This welding method does not produce the typical welding faults since the fusibility temperature is not achieved. The major problems of fusion welding in molybdenum are grain coarsening and irregular distribution of impurities along grain boundaries which can be mitigated to some extent by RFW [1]. RFW generates heat by producing relative movements between the connected partners, resulting in friction. It allows for the joining of materials with different compositions [2,3] as well as materials with high melting points, such as [4].

Friction welding techniques, such as friction stir welding (FSW) and RFW, were investigated for joining steel and aluminum alloys. The majority of the authors focused on joining steel/alloy plates using FSW with great concern for the formation of Intermetallic Compound (IMCs). Das *et al.* [5] reported that moderate IMCs were obtained by controlling energy input to improve the joint strength of the FSW lap joint between a 6063 Al alloy and zinc-coated steel. Pourali *et al.* [6] found a layer of IMCs with a thickness of 93 μm in the FSW lap joint between St37 steel and Al, and they found that it had no effect on joint strength. Shen *et al.* [7] reported that as penetration depth increased, few IMCs of $\text{Fe}_4\text{Al}_{13}$ developed at the interface of lap joint between aluminum 5754 Al alloy and steel DP600 dual-phase, enhancing the joint strength. Moreover, Hao *et al.* [8] studied the continuous drive friction welding of aluminum alloy 6061 and austenitic stainless steel 304 under different welding parameters, and they found that joining the alloy and stainless steel could be satisfactorily bonded. When no detection was present at the interface, sound welded connections with a joint efficiency of 88 percent and bending angles of 80

degrees were obtained at low friction and high upset pressure.

Aeronautic aluminum alloy 2024 was joined using CDFW. Geng *et al.* [9] examined the Parametric Optimization and Microstructural Characterization of the 2024 aluminum alloy. Excellent mechanical properties can be attributed to the sedimentation of reinforcement phases, such as Al₂Cu and Al₂CuMg, upon solid solution and artificial aging [10]. Conventional fusion welding often results in the formation of strengthening precipitates in the aluminum alloy weld throughout the thermal cycling of the welding process leads to the growth. The solidification cracks, coarse grain porosities, and slag inclusions present in fusion welding aluminum alloys make it difficult to obtain a sound welded joint [11-13]. Friction welding techniques, such as RFW, FSW, and linear friction welding, were introduced and used to join the various aluminum alloys were studied by MA, *et al.* [14] as a result of the technical advantages of solid-state welding, such as refined microstructure and no solidification. It is also investigated whether Al can be joined to different alloys, such as Copper [15], carbon steels [16], and titanium alloys [17]. There was also an investigation of the effect of friction time on the mechanical properties of titanium-stainless steel welding [18]. Tashkandi, *et al.* [19] assessed the effects of friction duration on the structure of AA6061 joints produced using CDFW, as well as the relation between the microstructure and thermal properties. Bharathi, *et al.* [20] studied the fusion of dissimilar aluminum alloys at various rotational speeds of 1100 and 1200 rpm and discovered that the joints formed at higher speeds had an 85% success rate.

In the present research, the effect of several operational parameters, such as the change in rotational speed and friction time with the change in applied forces, on the dynamic performance of AL6061 friction welded joints was studied. The experimental analyses were investigated by using two techniques. The first is the frequency response function method (FRF), which uses an impact hammering test, and the second is an ultrasonic technique that uses the magneto strictive pulse-echo delay-line for friction welded joint characterization.

2. Problem Description

Various friction welding joints were produced for aluminum alloy 6061 rods with a diameter of 14 mm and a length of 50 mm. The chemical compositions of aluminum alloy (6061 AA) have been detected by Optical Emission Spectrometer (OES) as presented in Table 1 according to Wang *et al.* [21]. Before welding, all contacting surfaces of workpieces were polished with a surface grinding machine. The mechanical properties of the aluminum alloy (6061 AA) are listed in Table 2. [22].

Table 1- Chemical compositions of 6061 AA (wt. %).

Material	AL	Mg	Si	Fe	Cu	Ni
6061AA	Bal.	0.9	0.75	0.5	0.5	0.05
Material	Cu	Mn	Zn	Cr	Ti	
6061AA	0.5	0.13	0.03	0.03	0.15	

Table 2- Mechanical properties of base alloy 6061 AA

Yield strength (MPa)	Tensile strength (MPa)	'Vicker's Hardness (Hv)	Elongation (%)
276	310	107	17

The CDFW machine was utilized to tow weld aluminum alloy rods. The rotating side received the first aluminum alloy rod, while the stationary side received the second rod. The joints were welded under different friction forces of 15 and 20 N with two distinct rotational speeds of 1100 and 1400 rpm and several upset times of 6, 8, and 10 sec. A schematic elucidation of the friction welding process and geometry of the welded specimens is shown in Fig. 1.

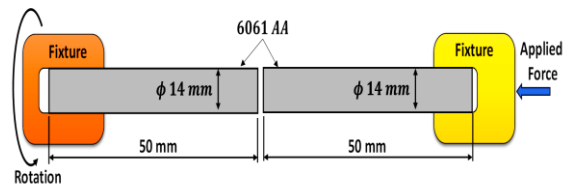


Figure 1- Schematic elucidation of rotating friction welding process.

3. Description of Friction Welding Machine

The lathe machine "G-400E Medium Duty Centre Lathe" was capable of great precision operating and repeatability across all weld parameters. The spindle was driven by an AC spindle motor. This machine was upgraded by upsetting forces are measured by a load cell and accurately controlled by a hydraulic servo valve. The machine is controlled by a single computer, which records the data of each weld.

Figure 2 shows the machine with a stroke of 300 mm and a maximum upset force of 20 N. The spindle motor was about 20 HP, 3 phase AC and operating speed can be varied from 82 to 2000 rpm.



Figure 2- G-400E Medium Duty Centre Lathe.

4. Finite Element Modeling

Finite element modeling was carried out by using SOLIDWORKS 2016 software. The fine mesh setup has been completed in the welded region. The finite element models, along with operating conditions for CDFW, are shown in Fig. 3. The welded joint of a typical aluminum bar with CDFW joint of dimensions 100 mm long and 14 mm diameter is simulated with various friction times, three types of rotational speed, and two forces. The mechanical properties of CDFW joint material are listed in Table 3.

According to Table 4, the maximum error between the theoretical and experimental values is within (4.55%), the lowest value is (1.07%), and the average error does not exceed (2.7%).

The dynamic equations of motion of CDFW for (6061AA) circular rod structure can be derived by using Lagrange equations and Hamilton's principle [23]. The Lagrange equations are given by

$$\frac{d}{dt} \left\{ \frac{\partial T}{\partial \dot{q}} \right\} - \left\{ \frac{\partial T}{\partial q} \right\} + \left\{ \frac{\partial V}{\partial q} \right\} = \{0\} \quad (1)$$

Where T is the kinetic energy, V is the potential energy, q is the nodal displacement, and \dot{q} is the nodal velocity.

The mass and stiffness matrix of the element can be formulated as,

$$[M] = \sum_{e=1}^E \iiint \rho [N]^T [N] dV \quad (2)$$

$$[K] = \sum_{e=1}^E \iiint [B]^T [N] [B] dV \quad (3)$$

Where $[M]$ is the element mass matrix, $[K]$ is the element stiffness matrix, ρ is the density, $[N]$ the matrix of shape functions, $[B]$ the matrix of coordinate derivatives of shape functions, and $[D]$ is the matrix of elastic constants.

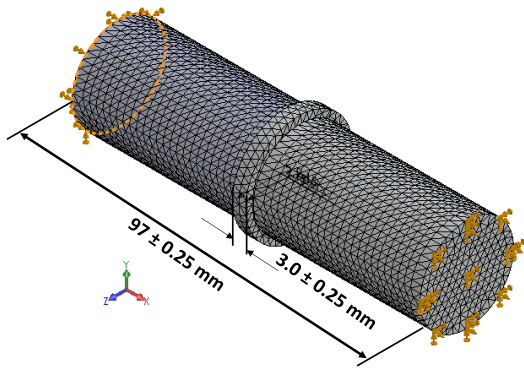


Figure 3- Finite element model for continuous drive friction welding joint.

By using the finite element method, the equation of motion of the system for an undamped vibration is given as

$$[M]\ddot{q}(t) + [K]q(t) = 0 \quad (4)$$

where $\ddot{q}(t)$ and $q(t)$ are the vectors of nodal accelerations and displacements,

The eigenvalue problem can be given by solving equation (4)

$$\det([K] - \gamma[M]) = \{0\} \quad (5)$$

According to Eq. (5), the program has been coded into a computer using SOLIDWORKS. The program computes the eigenvalues and eigenvectors for continuous drive friction welding joint, as shown in Table 4.

5. Experimental Work

5.1 Tensile Test

The aluminum alloy (6061 AA) was cut into the desired dimension, as shown in Fig. 4. The mechanical tensile test was performed according to ASTM standards EL-Wazerya *et al.* [24] using an electromechanically controlled universal testing machine (UH-F1000kN) with a crosshead speed of 5 mm/min. According to the ASTM standard, the specimens were loaded at the rate of 1.5 kN/min. All specimens were subjected to a tensile test, and their values were recorded.

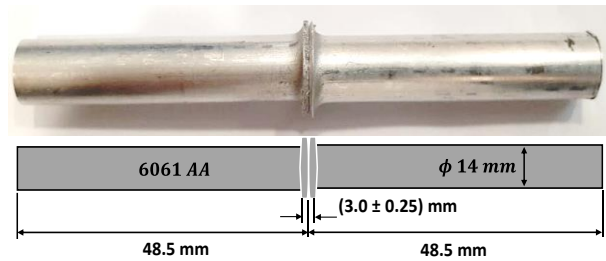


Figure 4- Tensile test specimens.

5.2 Dynamic Test

The experimental setup for measuring free vibration of the aluminum bars with continuous drive friction welding of 6061 Al alloy (6061AA) was tested and validated. These tests were accomplished using B&K tri-axial piezoelectric type (4506), B&K impact hammer type (8202) and B&K data acquisition type (3160), which connected to the computer as presented in Fig. 5. A comprehensive stand-alone analyzer test system is the setup of a collection of inputs and outputs. The module is ideal for electro-acoustic test applications and audio, as well as other applications that need system stimulation. The frequency range of all input and output channels is 20 to 51 kHz.

Fig. 6 shows the coherence and frequency response function recorded in a specimen welding joint of Al alloy (6061AA) at $t = 4$ sec, $F = 15$ N, $S = 1400$ rpm.

For measuring the natural frequencies of continuous drive friction welding of (6061AA), one end of the joint was clamped under heavy support. An electromagnetic accelerometer was connected to the joint at a distance of 20% of the length of the joint from the clamped end and very close to a free edge. At the anti-node point, an impact hammer is utilized to stimulate the specimen. The frequency response spectrum may be obtained from the printer, which is supported by the desktop computer series the dual-channel analyzer Ghoneam *et al.* [25].

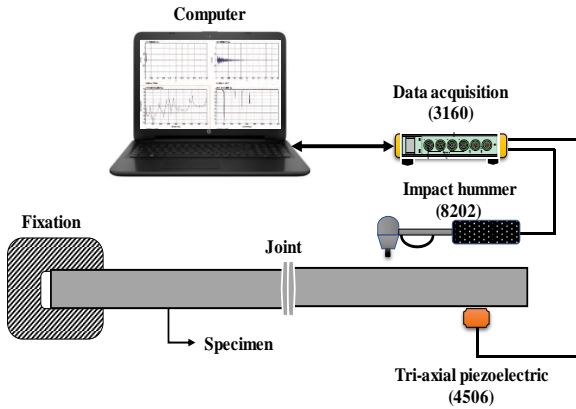


Figure 5- Schematic diagram of the setup used in the experimental tests.

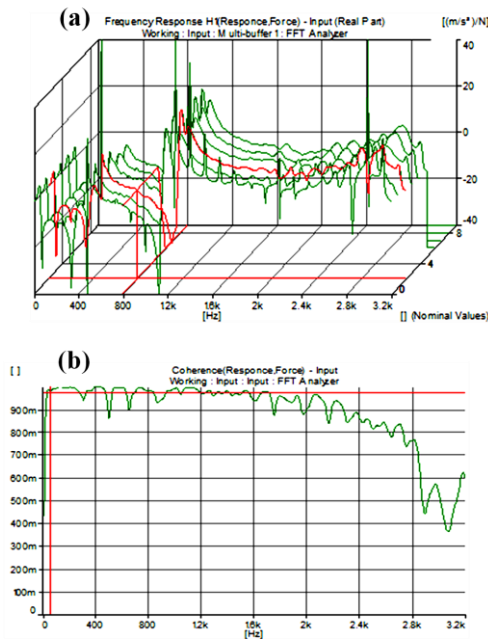


Figure 6- A sample of frequency response function and coherence function for continuous drive friction welding joint of Al alloy (6061AA) at $t_f = 4$ sec, $F = 15$ N, $S = 1400$ rpm.

6. Ultrasonic Measurements

6.1 Phase Velocity Measurements

Longitudinal ultrasonic velocity measurements were obtained using the pulse-echo method described in our earlier study [26] using a high-power ultrasonic pulse-echo receiver system and a 100 MHz digital storage oscilloscope (COS5020). Transducers were used to generate ultrasonic waves.

High precision transit times were measured using a cross-correlation technique. By measuring the transit times, t_0 in each specimen using the relationship [27] ultrasonic phase velocities v_p can be calculated as follows:

$$v_p = \frac{2L}{t_0} \quad (6)$$

Where L is the length of the sample and wire. Phase velocity was measured with an error of $\pm 1.1\%$.

Where \mathcal{A}_m is the maximum amplitude (voltage) of the m^{th} and \mathcal{A}_n is the n^{th} pulse echoes. The percentage error in the attenuation measurement was $\pm 2.1\%$. Fig. 7 illustrates the basic system used for these measurements.

6.2 Dynamic Young's Modulus

The most accurate dynamic Young's modulus (E_d) usually follows from determining ultrasonic v_p by using the general relationship [27], [28] given in equation (7).

$$E_d = \rho v_p^2 \frac{(1+v)(1-2v)}{(1-v)} \quad (7)$$

Where ρ is the denoted mass density and ν is 'Poisson's coefficient, assumed to be 0.33.

6.3 Attenuation Factor

The attenuation factor of ultrasonic waves was evaluated at a frequency of 5 MHz using a transducer of the contact type. According to our results with various couplants available for room temperature measurements, machine oil and honey are most suited for getting steady back wall echoes in the oscilloscope screen for longitudinal waves and shear waves. Utilizing the relation for the attenuation coefficient [27], the attenuation factor was determined by measuring the amplitude of successive back wall echoes from the welded joint.

$$\mathfrak{B} = \left(\frac{-10}{(m-n)L} \right) \log \frac{\mathcal{A}_m}{\mathcal{A}_n} \quad (8)$$

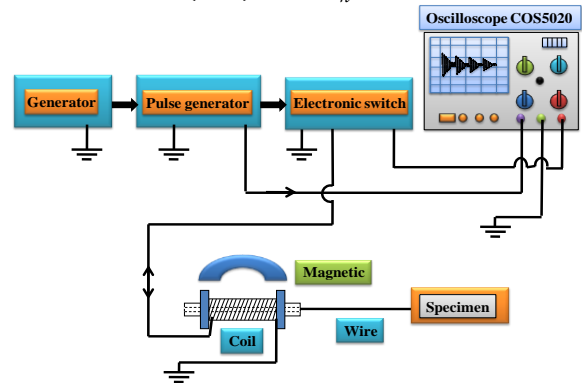


Figure 7- Schematic diagram of the magnetostrictive delay-line system.

7. Results and Discussion

The results include the analysis of the stress-strain curves, dynamic analysis (eigen parameters), and ultrasonic parameters for all welded samples as a function of friction time, rotational speeds, and applied force.

7.1 Tensile Properties

Figure 8 illustrated the relationship between the average engineering stress-strain (σ - ϵ) curve for AA6061 with friction time $t = 4$ sec and three different

values of rotational speed $S_1 = 1100$ rpm, $S_2 = 1400$ rpm, and $S_3 = 2000$ rpm, with two types of applied forces F (15 and 20 N). When comparing a sample with a speed of 1400 rpm has the largest value of yield strength σ_y and ultimate tensile stress UTS compared with a sample with a speed of 1100 rpm. These values are listed in Table 3.

For both applied forces with all friction time values, at 1400 rpm-rotational speed, the weld joint quality arises the highest yield and ultimate tensile strength. This may be explained by a suitable cooling rate and grain size. Conversely, the reduction in yield and ultimate tensile strength of welded joint produced a high temperature and low cooling rate at a rotational speed of 2000 rpm, followed by coarsening of grains. While the rotational speed of 1100 rpm caused a decrease in the rate of bonding between the particles in the welding zone due to a reduction in heat generation and faster cooling rate, resulting in a lower ultimate tensile strength.

The (σ - ϵ) curves for rotational speed 1400 and 2000 rpm at applied force 15 N appear to have relatively close σ_y and UTS values, as shown in Fig. 8. On the other hand, in the second (σ - ϵ) curve at the force 20 N, the convergence between the values of σ_y and UTS at speeds 1100 and 1400 rpm was due to the change in the value of the force acting on the welded joint.

The properties of the friction welded joints depend on the rotational speed, friction time, and applied force. Tensile properties of the friction welded joint were mostly affected by the materials and specimen conditions. From Table 3, the value of the stress UTS was increased by 18.7% as a result of the change in rotational speed from 1100 to 1400 rpm at the friction time of 4 sec and effective force of 15 N, while the stress was decreased by 10.97% when the rotational speed changed from 1400 to 2000 rpm. Hence, we noted that the maximum value of the UTS stress was obtained at a speed of 1400 rpm, compared to 1100 and 2000 rpm speeds, and this is due to the temperatures generated by the welding process.

We can also see from Table 3 that UTS was decreased with an increase in friction time. At a rotational speed of 1400 rpm and applied force of 15 N, the stress was decreased by 10.9% when the friction time changed from 4 to 6 sec, while it was decreased by 14.44% when the time changed from 6 to 8 sec. The force changed from 15 to 20 N at a friction time of 4 sec, and at a rotational speed of 1400 rpm, the stress UTS was decreased by 14.82%.

Figure 8(a, b) shows that the ultimate tensile strength increased when the rotational speed was increased from 1100 to 1400 rpm and then slightly decreased when the rotational speed became 2000 rpm, but it was still higher than that of at 1100 rpm. Increasing the load from 15 to 20 N resulted in lowering the ultimate tensile values.

7.2 Dynamic Analysis

The resonance frequency of AA6061 bar with rotating CDFW has been recorded with three types of friction time and different types of rotational speed, and it has also been analyzed for different applied forces. The measured and the computed fundamental frequencies are shown in Table 4. The experimental results verified the numerical values obtained from the solution of Eq. 5. The numerical results of the present study are in good compatibility with the experimental results. From Fig. 9(a) and (b), it can be observed that the sample with a speed of 1100 rpm has the lowest frequency compared with the other specimen while the sample with a speed of 1400 rpm has the highest values, such effect may be due to the minimum and maximum values of flexural elastic modulus and stiffness at this applied force, respectively. On the other hand, in Fig. 9(a), the friction time of 4 sec has the maximum values of the fundamental frequency, whereas the friction time of 8 sec has minimum values of frequency simply due to the low value of applied force (15 N).

From Fig. 9(b), it can be seen that the friction time of 6 sec has the maximum values of the fundamental frequency. In contrast, the friction time of 8 sec has minimum values of frequency, and this is due to the effect of a low level of potential energy at this time.. Given different rotational speeds, the rate of change of the Eigen-frequencies via different rotational speeds is relatively high compared to the rate of change due to the use of the various friction times, as shown in Fig. 9. From Table 4, by changing the applied force from 15 to 20 N, the frequency decreased by 38.3% at a friction time of 4 sec and rotational speed 1100 rpm, and when the friction time was changed from 4 to 6 sec at the same rotational speed (1100 rpm), the fundamental natural frequency decreased by 5.5%. Hence, it becomes clear that the applied force acting on the welded joint has more influence than the friction time on the fundamental natural frequency.

As presented in Table 4, the maximum value of the damping factor was achieved at the rotational speed of 1000 rpm, while the lowest value of the damping factor was at 1400 rpm. The reason is that the damping coefficient is inversely proportional to the value of the natural frequency of the welding area.

In addition, for a given value of rotational speed and 15 N applied force Fig. 9(a), the frequency increases linearly with time values with the correspondent increase in strength and the decrease in damping. This friction depends on time as reflectors by homogeneity in deformation and the acceleration in dynamic recrystallization. Thus, the grains refinement improves, and their distribution in precipitates becomes better.

On the other hand, from Fig. 10 and Table 4, the damping factor increased monotonically as the friction time reached a maximum at the applied force of 20 N, and the reason is due to maximum dissipated energy at this force. These differences mainly depend on the

bonding strength of the linkage molecules in the weld region due to the effect of applied force.

According to Fig. 10(a), for an applied force of 15 N, the highest damping factor is found at a speed of 1100 rpm, while 1400 rpm had the lowest damping factor. Similarly, when the time changed from 4 to 8 sec, we observed that the damping factor had the highest value at 8 sec and the lowest at 4 sec. This phenomenon is because the dissipation energy is higher at an 1100 rpm rotational speed and an 8 sec friction time.

According to Fig. 10(b), the damping factor at speed 1100 rpm had the highest value, whereas the damping factor at speed 1400 rpm had the lowest value. Concerning the effect of friction time on the damping factor, the highest value was obtained at 8 sec and the lowest value at 6 sec, which is due to the greater dissipation energy at 1100 rpm, and 8 sec time, respectively.

The present comparison between the numerical method (using the finite element method) and experimental results proves that the suggested finite element models of the rotating CDFW joint specimens provide an efficient tool for computing the dynamic analysis with proper accuracy.

Thus, the frequency and damping factor level can be controlled by changing the applied force, friction time, and rotational speed, and consequently, the results obtained are beneficial for the designer to select the properly applied force, friction time, and rotational speed.

At a specific value of friction time and applied force, frequency increases with rotational speed, reaches a maximum, and then decreases. The increase in frequency may be related to the increase in stiffness with the resultant drop in damping. On the other hand, high rotational speed results in microstructural defects that result in a drop in frequency but an increase in damping.

7.3 Ultrasonic Results

The propagation of the ultrasonic phase velocity in the specimen v_p , the dynamic elastic modulus E_d , and attenuated factors \mathfrak{B} for the first two echoes are given in Table 5.

It is observed that the obtained results for E_d and v_p are found to be symmetrical. In every welded joint specimen, a maximum value of E_d corresponds to a minimum attenuation factor, as presented in Table 5.

From Fig 11 (a & b), it can be seen that the specimen with friction time 4 sec and rotational speed 1400 rpm at applied force 15 N and the specimen with friction time 6 sec and rotational speed 1400 rpm at applied force 20 N had the highest value of dynamic young's modulus E_d , compared with the other specimens. This is because the value of sound velocity is higher at these conditions than in other samples.

From Fig. 11(a), we found that there was convergence in the values of dynamic young's modulus at the time of 8 sec, while at the time of 4 sec, there was a divergence in the values of dynamic young's. This is because, at a time of 4 sec, the wave propagation path can pass easily through the welding area, and there is no disturbance of the wave propagation path there. Moreover, the welding area has better properties than other times.

Attenuation factor, rotational speed, and friction time are correlated in Fig. 12. A greater attenuation factor was observed at a rotational speed of 1100 rpm, while a lower value at a rotational speed of 1400 rpm, and this is because the dissipation energy at a rotational speed of 1100 rpm is higher than that of 1400 rpm.

From Fig 12(a), it can be seen that the specimen with friction time of 8 sec and rotational speed 1100 rpm has the highest value of attenuation factor compared with the other specimens with friction time of 4 sec and rotational speed 1400 rpm. Additionally, from Fig 12(b), the highest value of attenuation factor was found at time 8 sec and 1100 rpm rotational speed compared with the specimen with 6 sec and 1400 rpm rotational speed that has the lowest value. This is because wave propagation in the welding area is slower at friction time of 8 sec and rotational speed of 1100 rpm than in the other samples.

According to Fig. 12(b), for a friction time of 4 sec, there is a divergence in the values of the attenuation factor with the change in rotational speed, whereas, for a friction time of 8 sec, there is convergence in the values of the attenuation factor with the change in rotational speed. This phenomenon occurs because the crystal structure of the material at the weld area changes as the friction time increases.

Obviously, the produced overlapped welding zone effects with the applied force, rotational speed, the two-rod material type, the contact area, the contact time up to the formation of the welding zone, and the nature of the surrounding environment. The cooling rate of the highly heated overlapped zone may also affect the process.

All of these aforementioned parameters can change the nature of the produced overlapped welding zone. In this zone, some factors, such as the maximum maintained temperature, the rate of oxidation (due to reaction with a surrounding environment, especially oxygen), the rate of recrystallization, and solidification of the overheated overlapped contact zone just before welding can affect the physical and chemical nature of the overlapped zone produced.

Hence, the characteristics of sound wave propagation inside such zone can be changed and different from those used contact rods.

Table 3- Mechanical properties retained from the stress-strain curves.

Sample No.	Applied Force, F [N]	Time, t [sec]	Rotational Speed, S [rpm]	Yield strength, σ_y [MPa]	UTS, σ_u [MPa]	
1	15	4	1100	55.42	112.33	
2			1400	73.12	133.43	
3			2000	64.34	120.24	
4		6	6	1100	50.21	110.41
5				1400	68.51	120.33
6				2000	58.42	117.22
7			8	1100	47.23	95.11
8				1400	67.34	105.14
9				2000	57.12	99.44
10	20	4	1100	48.12	95.42	
11			1400	68.43	112.14	
12			2000	61.32	103.44	
13		6	6	1100	44.34	98.51
14				1400	59.44	116.21
15				2000	52.34	108.11
16			8	1100	41.51	90.12
17				1400	59.13	103.24
18				2000	52.22	94.31

Table 4- Fundamental natural frequency in Hz at various fraction times in s, three types of rotational speed and different forces.

Sample No.	Applied Force, F [N]	Time, t [sec]	Speed, S [rpm]	Natural frequency, f [Hz]		Damping ξ	
				EX	FE		
1	15	4	1100	125.51	128.14	0.184	
2			1400	131.81	136.43	0.131	
3			2000	128.41	132.02	0.154	
4		6	6	1100	119.81	121.11	0.213
5				1400	126.44	129.21	0.163
6				2000	123.02	125.01	0.182
7			8	1100	87.34	90.12	0.262
8				1400	119.51	122.33	0.195
9				2000	113.82	115.41	0.232
10	20	4	1100	77.31	79.12	0.351	
11			1400	99.42	104.23	0.223	
12			2000	92.12	95.04	0.315	
13		6	6	1100	86.14	88.43	0.274
14				1400	111.21	114.24	0.198
15				2000	98.71	103.42	0.251
16			8	1100	74.02	75.15	0.421
17				1400	95.12	98.43	0.382
18				2000	86.44	90.21	0.411

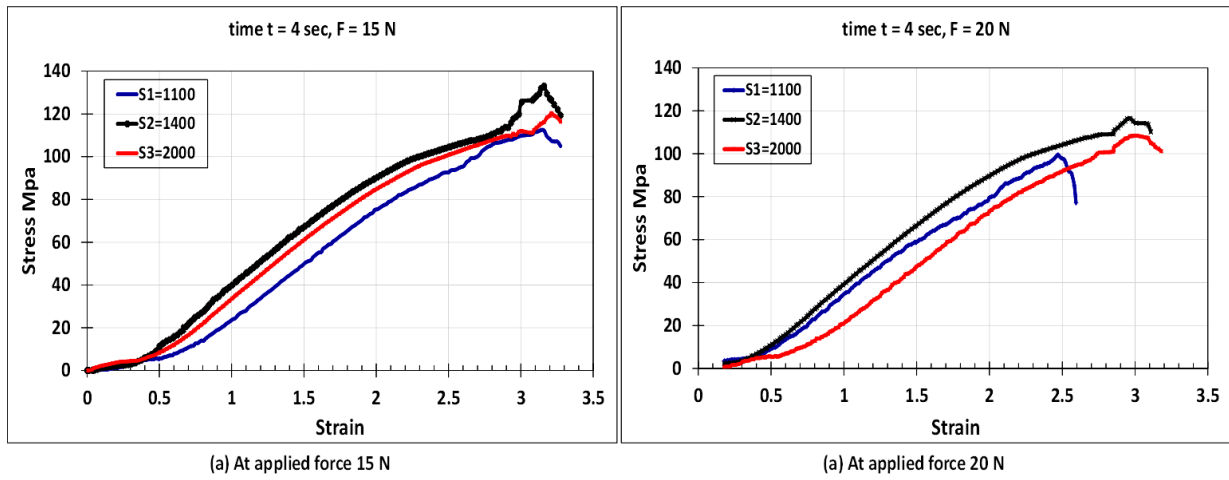


Figure 8- Engineering stress vs. engineering strain as a function of friction time, applied forces, and rotational speed of 1400 rpm.

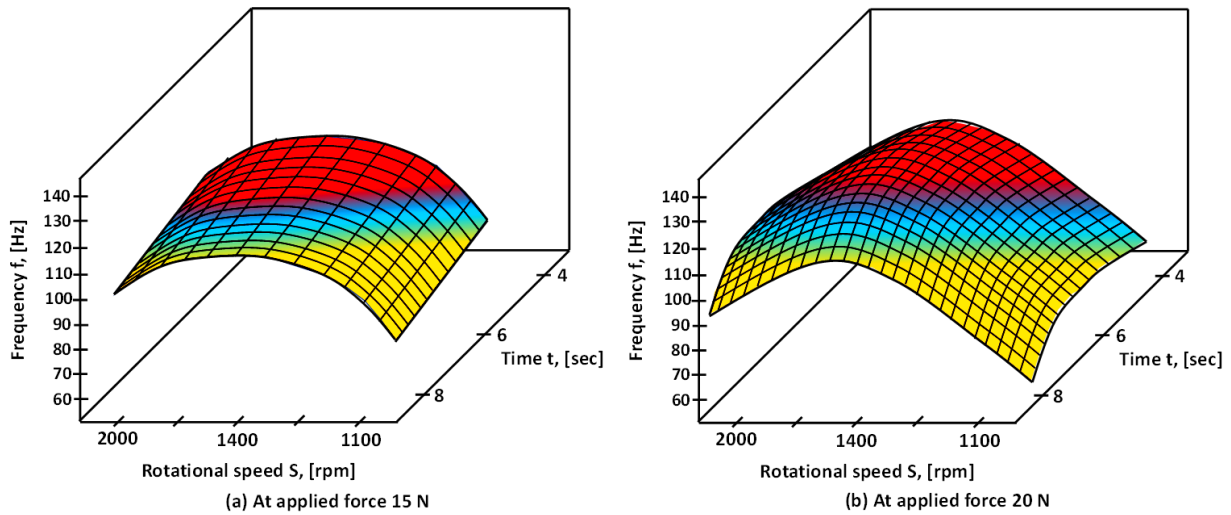


Figure 9- The relationship between natural frequency, rotational speed, and friction time.

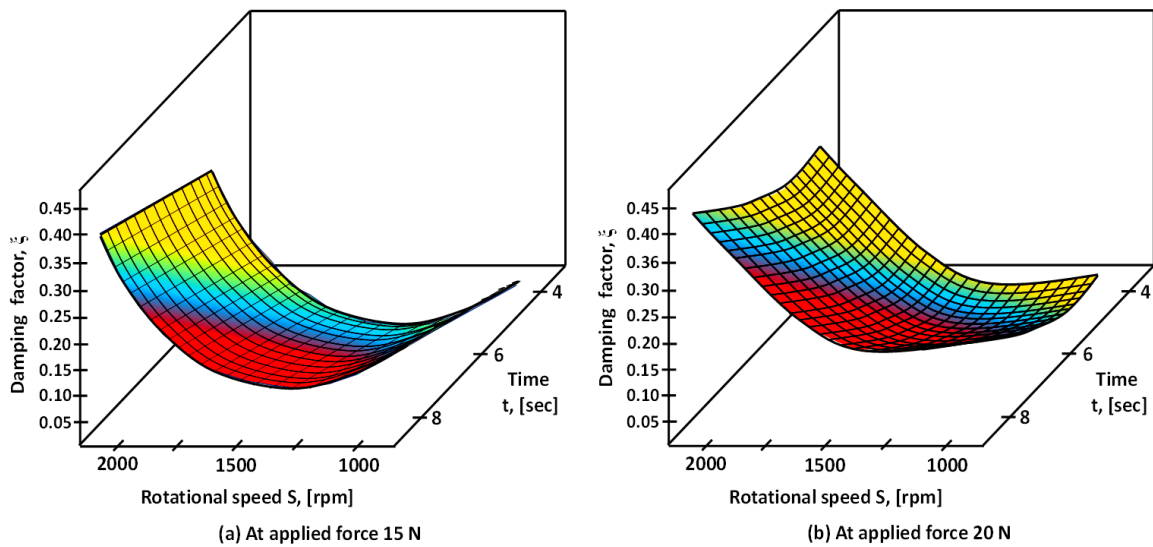


Figure 10- The relationship between damping factor, rotational speed, and friction time.

Table 5- Ultrasonic measurements.

Sample No.	Applied Force, F [N]	Time, t [sec]	Rotational Speed, S [rpm]	v_p , [m/sec]	E_d , [Gpa]	Attenuation Factor, β
0		Reference Material		6340	73.2	0.00528
1	15	4	1100	5491.3	54.9	0.00123
2			1400	5597.5	57.1	0.00087
3			2000	5561.2	56.4	0.00103
4		6	1100	5482.4	54.8	0.00137
5			1400	5566.3	56.5	0.00105
6			2000	5538.1	55.9	0.00117
7		8	1100	5443.1	53.9	0.00177
8			1400	5485.1	54.8	0.00132
9			2000	5462.1	54.3	0.00157
10	20	4	1100	5362.1	52.4	0.00225
11			1400	5410.1	53.3	0.00143
12			2000	5387.1	52.8	0.00202
13		6	1100	5420.4	53.3	0.00196
14			1400	5451.1	54.1	0.00141
15			2000	5434.1	53.8	0.00179
16		8	1100	5324.1	51.65	0.00301
17			1400	5385.1	52.8	0.00263
18			2000	5353.3	52.2	0.00284

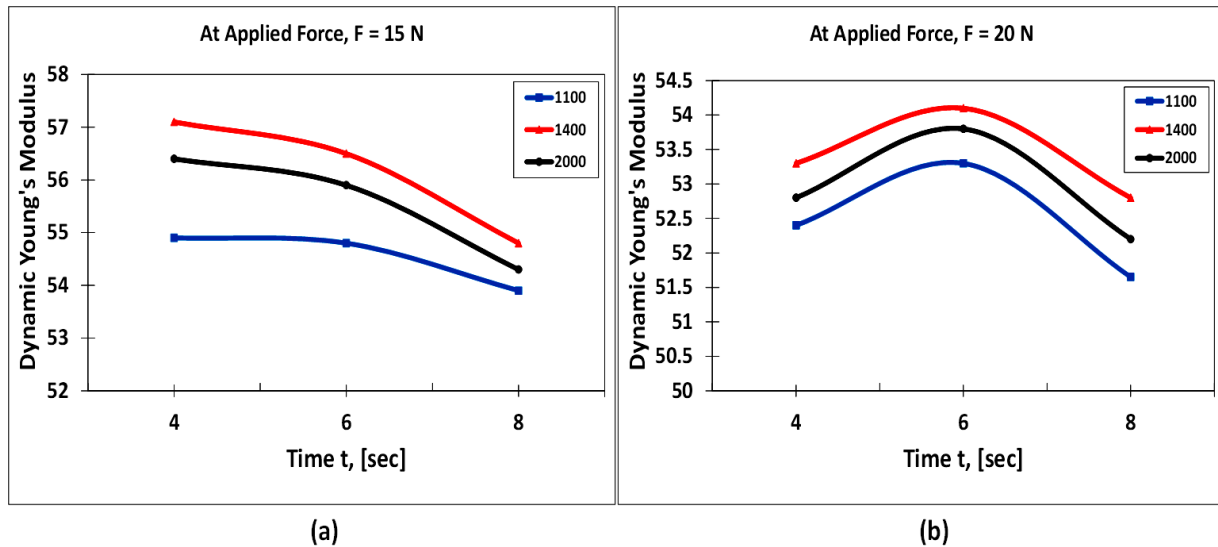


Figure 11- The relationship between dynamic young's modulus, rotational speed, and friction time.

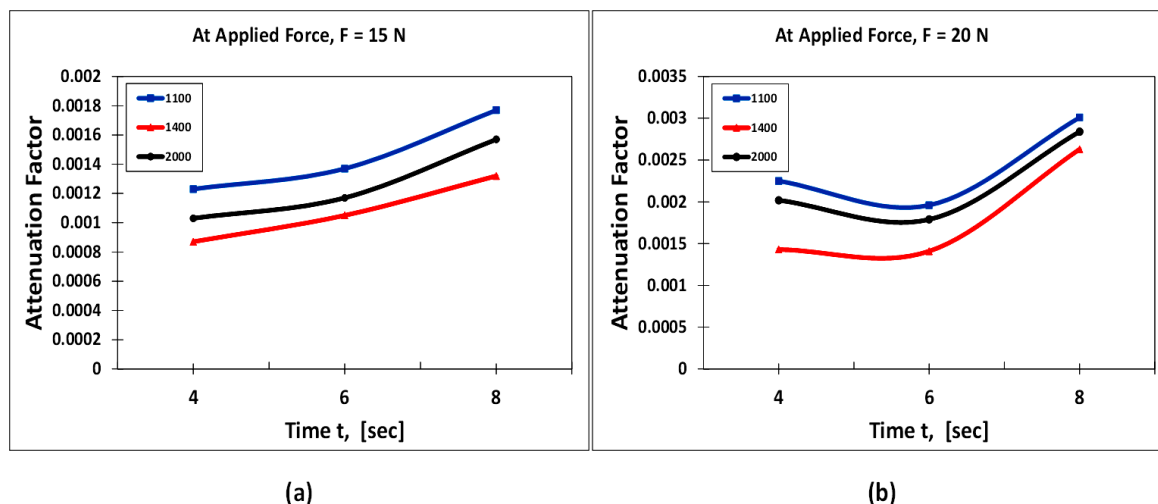


Figure 12- The relationship between attenuation factor, rotational speed, and friction time.

8. Conclusion

The dynamic analysis of rotating CDFW joint for an aluminum bar with different friction times, three levels of rotational speed, and two different types of applied force are investigated analytically and experimentally, where the following remarks are concluded:

1. The natural frequency rate is reduced by increasing both applied force and the friction time. When the applied force was increased by 33% at a friction time of 4 sec, the natural frequency of rotating CDFW joint was decreased by an average of 44.8%, while at the friction time of 6 sec, the natural frequency was decreased by 34.14%, and at the friction time of 8 sec, the natural frequency rate was reduced by 25.1%.
2. The maximum values of the frequency rate are obtained at rotational speed of 1400 rpm. The maximum value of frequency reached 131.81 Hz at friction time 4 sec when applying a force of 15 N and reached 111.21 Hz at friction time 6 sec when applying a force of 20 N.
3. The strength of the joints varied a little progressively when the friction time exceeded 4 sec. The highest strength could arrive up to 133.43 MPa on average when friction time was 4 sec at rotational speed 1400 rpm for applied force 15 N. Meanwhile, this value decreased to 150 MPa when the friction time was increased to 8 sec for 1400 rpm, at the same applied force.
4. The damping capacity is always inversely proportional to the stiffness of the rotating CDFW joint specimens. By changing the applied force to 33.3%, the damping factor was increased by 38.45%. On the other hand, the damping factor increased by 18.9%, when changing the friction time by 50%. The changing of the rotational speed from 1100 to 1400 rpm decreases the damping factor by 28.8% while the changing it from 1400 to 2000 rpm, increases the damping factor by 14.9%.
5. The non-destructive ultrasonic technique showed success when used for predicting the dynamic properties of a rotating CDFW joint for the 6061-aluminum alloy.

6. For CDFW joint of 14 mm-diameter 6061-aluminum bars, with using an applied force varying between 15 to 20 N, the dynamic young's modulus decreased by 4.7%, while the attenuation factor increased by 31.2%.

9. References:

- [1] M. Stütz, R. Buzolin, F. Pixner, C. Poletti, N. Enzinger, "Microstructure Development of Molybdenum During Rotary Friction Welding", *Materials Characterization*, Vol. 151, 2019, pp. 506–518.
- [2] M. Meisnar, S. Baker, J.M. Bennett, A. Bernad, A. Mostafa, S. Resch, N. Fernandes, A. Norman, "Microstructural Characterisation of Rotary Friction Welded AA6082 and Ti-6Al-4V Dissimilar Joints", *Materials and Design*, Vol. 132, No. 5, 2017, pp.188–197.
- [3] X. Li, J. Li, Z. Liao, F. Jin, F. Zhang, J. Xiong, "Microstructure Evolution and Mechanical Properties of Rotary Friction Welded TC4/SUS321 Joints at Various Rotation Speeds", *Materials and Design*, Vol. 99, No. 5, 2016, pp. 26–36.
- [4] A. Ambroziak, "Friction Welding of Molybdenum to Molybdenum and to Other Metals", *International Journal of Refractory Metals and Hard Materials*, Vol. 29, No. 4, 2011, pp. 462–469.
- [5] H. Das, S. Basak, G. Das, TK. Pal, "Influence of Energy Induced from Processing Parameters on the Mechanical Properties of Friction Stir Welded Lap Joint of Aluminum to Coated Steel Sheet", *Int Journal of Advanced Manufacturing Technology*, Vol. 64, 2013, pp. 1653-1661.
- [6] M. Pourali, A. Abdollah-zadeh, T. Saeid, F. Kargar, "Influence of Welding Parameters on Intermetallic Compounds Formation in Dissimilar Steel/Aluminum Friction Stir Welds", *Journal of Alloys Compounds*, Vol. 715, No. 25, 2017, pp 1-8.

- [7] Z. Shen, Y. Chen, M. Haghshenas, AP. Gerlich, "Role of Welding Parameters on Interfacial Bonding in Dissimilar Steel/Aluminum Friction Stir Welds", *Engineering Science and Technology, an International Journal*, Vol. 18, No. 2, 2015, pp. 270-277.
- [8] W. Hao, Q. Guoliang, G. Peihao, M. Xiaofei, "Interfacial Microstructures and Mechanical Properties of Friction Welded Al/Steel Dissimilar Joints", *Journal of Manufacturing Processes*, Vol. 49, 2020, pp. 18–25.
- [9] P. Geng, G. Qin, J. Zhou, C. Li, "Parametric Optimization and Microstructural Characterization of Friction Welded Aeronautic Aluminum Alloy 2024", *Transactions of Nonferrous Metals Society China*, Vol. 29, No. 12, 2019, pp. 2483–2495.
- [10] J. L. Gu, J. Bai, J. L. Ding, S. Williams, L. Wang, K. Liu, W. Stewart, L. Wang Li-min., "Design and Cracking Susceptibility of Additively Manufactured Al–Cu–Mg Alloys with Tandem Wires and Pulsed Arc", *Journal of Materials Processing Technology*, Vol. 262, 2018, pp. 210–220.
- [11] S. R. K. Rao, G. M. Reddy, M. Kamaraj, K. P. Rao, "Grain Refinement Through Arc Manipulation Techniques in Al–Cu Alloy GTA Welds", *Materials Science and Engineering A*, Vol. 404, No. (1–2) , 2005, pp. 227–234.
- [12] J. Yan, X. Y. Zeng, M. Gao, J. Lai, T. Lin, "Effect of Welding Wires on Microstructure and Mechanical Properties of 2A1₂ Aluminum Alloy in CO₂ Laser-MIG Hybrid Welding", *Apply Surface Science*, Vol. 255, No. 16, 2009, pp. 7307–7313.
- [13] V. Balasubramanian, V. Ravisankar, G. M. Reddy, "Effect of Pulsed Current Welding on Fatigue Behaviour of High Strength Aluminum Alloy Joints", *Material & Design*, Vol. 29, No. 2, 2008, pp. 492–500.
- [14] H. Ma, G. L. Qin, P. H. Geng, F. Li, B. L. Fu, X. M. Meng, "Microstructure Characterization and Properties of Carbon Steel to Stainless Steel Dissimilar Metal Joint Made by Friction Welding", *Material & Design*, Vol. 86, No. 5, 2015, pp. 587–597.
- [15] M. Sahin, "Joining of aluminium and copper materials with friction welding", *International Journal of Advanced Manufacturing Technology*, Vol. 49, No. (5-8) , 2010, pp. 527–534.
- [16] T. C. Nguyen, D. C. Weckman, "A thermal and microstructure evolution model of direct-drive friction welding of plain carbon steel", *Metallurgical and Materials Transactions B*, Vol. 37, No. 2, 2006, pp. 275–292.
- [17] M. A. Tashkandi, J. A. Al-jarrah, M. Ibrahim, "Spot welding of 6061 Aluminum alloy by friction stir spot welding process", *Engineering Technology & Applied Science Research*, Vol. 7, No. 3, 2017, pp. 1629-1632.
- [18] J. A. Al-jarrah, A. Ibrahim, S. Sawlaha, "Effect of applied pressure on mechanical properties of 6061 Aluminum alloy welded joints prepared by friction stir welding", *Engineering, Technology & Applied Science Research*, Vol. 7, No. 3, 2017, pp. 1619-1622.
- [19] M. A. Tashkandi and M. I. Mohamed, "Effect of Friction Time on the Mechanical and Microstructural Properties of AA6061 Joints by Continuous Drive Friction Welding", *Engineering, Technology & Applied Science Research*, Vol. 10, No. 3, 2020, pp. 5596-5602.
- [20] SRS. Bharathi, R. Rajeshkumar, A.R. Rose, and V. Balasubramanian, "Mechanical Properties and Microstructural Characteristics of Friction Welded Dissimilar Joints of Aluminium Alloys", *Materials Today: Proceedings*, Vol. 5, No. 2, 2018, pp. 6755–6763.
- [21] H. Wang, G. Qin, P. Geng, X. Ma, "Interfacial Microstructures and Mechanical Properties of Friction Welded Al/Steel Dissimilar Joints", *Journal of Manufacturing Processes*, Vol. 49, 2020, pp. 18–25.
- [22] M. Vigneshwar, S. T. Selvamani, P. Hariprasath, K. Palanikumar, "Analysis of Mechanical, Metallurgical and Fatigue Behavior of Friction Welded AA6061-AA2024 Dissimilar Aluminum Alloys in Optimized Condition", *Materials Today: Proceedings*, Vol. 5, No. 2, 2018, pp. 7853–7863.
- [23] JN. Reddy, "Introduction to the Finite Element Method", 3rd ed. New York: McGraw-Hill College, 2005.
- [24] M. S. EL-Wazerya, M. I. EL-Elamy, and S. H. Zoalfakar, "Mechanical Properties of Glass Fiber Reinforced Polyester Composites", *International Journal of Applied Science and Engineering*, Vol. 14, No. 3, 2017, pp. 121-131.
- [25] S. M. Ghoneam, A. A. Hamada and M. I. EL-Elamy, "Experimental and Analytical Investigations of the Dynamic Analysis of Adhesively Bonded Joints for Composite Structures", *Solid State Phenomena*, Vol. 147-149, 2009, pp. 663-675.
- [26] V. Rajendran, N. Palanivlu, P. Palanichamy, T. Jayakumar, Baldev Raj and B. K. Chaudhuri, " Ultrasonic characterization of ferroelectric BaTiO₃ doped lead bismuth oxide semiconducting glasses", *Journal of Non-Crystalline Solids*, Vol. 296, 2001, pp. 39-49.
- [27] V. Rajendran, A. V. Gayathri Devi, M. Azooz, F. H. El-Batal, "Physicochemical studies of phosphate based P₂O₅-Na₂O-CaO-TiO₂ glasses for biomedical applications", *Journal of Non-Crystalline Solids*, Vol. 353, 2007, pp. 77-84.
- [28] W. A. Thomaz, D. Y. Miyaji, and E. Possan, "Comparative study of dynamic and static Young's modulus of concrete containing basaltic aggregates", *Case Studies in Construction Materials*, Vol. 15, 2021, pp. 1-17.